Experimental Mechanics (2007) 47:451–463
DOI 10.1007/s11340-006-9007-7

Miniaturized Compression Test at Very High Strain Rates by Direct Impact

J.Z. Malinowski · J.R. Klepaczko · Z.L. Kowalewski

Received: 11 January 2005 / Accepted: 5 August 2006 / Published online: 2 March 2007
© Society for Experimental Mechanics 2007

Abstract A modified miniaturized version of the Direct Impact Compression Test (DICT) technique is described in this paper. The method permits determination of the rate-sensitive plastic properties of materials up to strain rate $\sim 10^5$ s^{-1}. Miniaturization of the experimental setup with specimen dimensions: diameter d_S=2.0 mm and thickness l_S=1.0 mm, Hopkinson bar diameter 5.2 mm, with application of a novel optical arrangement in measurement of specimen strain, makes possible compression tests at strain rates from $\sim 10^3$ s^{-1} to $\sim 10^5$ s^{-1}. In order to estimate the rate sensitivity of a low-alloy construction steel, quasi-static, Split Hopkinson Pressure Bar (SHPB) and DICT tests have been performed at room temperature within the rate spectrum ranging from $5*10^{-4}$ s^{-1} to $5*10^4$ s^{-1}. Adiabatic heating and friction effects are analyzed and the final true stress versus true strain curves at different strain rates are corrected to a constant temperature and zero friction. The results have been analyzed in the form of true stress versus the logarithm of strain rate and they show two regions of a constant rate sensitivity $\beta = \left(\Delta\sigma \Big/ \log \dot{\varepsilon}\right)_{\varepsilon}$: relatively low up to the strain rate threshold ~50 s^{-1}, and relatively high above the threshold, up to strain rate $\sim 4.5*10^4$ s^{-1}.

J.Z. Malinowski · Z.L. Kowalewski
Institute of Fundamental Technological Research,
Polish Academy of Sciences,
21 Swietokrzyska St.,
00049 Warsaw, Poland

J.R. Klepaczko (✉)
Laboratory of Physics and Mechanics of Materials,
UMR-CNRS 7554, Metz University,
Ile du Saulcy,
57045 Metz, France
e-mail: Klepaczko@lpmm.univ-metz.fr

Keywords Direct Impact Compression Test (DICT) · Dynamic plasticity · Mild Steel · High strain rate

Introduction

It is well known that experimental determination of mechanical properties of materials at high strain rates is a difficult problem. It has also been known for a long time that most materials are dependent on the rate of deformation and temperature. Other factors are strain rate, temperature history effects, and microstructure. At strain rates above $\sim 10^3$ s^{-1}, the rate sensitivity for most metals and alloys substantially increases and an accurate and complete picture is necessary in formulation of constitutive relations in the range of the strain rate spectrum up to $\sim 10^6$ s^{-1}.

Although advances in electronics and recordings of short time processes have made it so that compression impact experiments are much easier at present to perform, some improvements in both mechanical design and measuring techniques are possible. One possibility is miniaturization of experimental set-ups. The miniaturization enables for a substantial increase of strain rate and also for reduction of the radial and longitudinal inertia of specimen. The miniaturization concepts have been employed in this study in order to reach strain rates up to $\sim 10^5$ s^{-1}.

One of the most popular experimental techniques applied in determination of visco-plastic properties of materials at strain rates from $\sim 5*10^2$ s^{-1} to $\sim 10^4$ s^{-1} is the Kolsky apparatus [1] or called Split Hopkinson Pressure Bar (SHPB). A modified version of the Kolsky apparatus, presently used in most laboratories, was developed by Lindholm [2]. In both versions, a wafer specimen is placed between bars. Such experimental technique can be applied in many configurations, for example in compression [3, 4],

tension [5, 6], torsion [7, 8], in shear [9, 10], and also in different sizes. In the case of the compression test, the disk specimens are prone to friction and inertia. Moreover, the use of the SHPB technique is limited by the elastic limit of the incident bar. According to the one-dimensional elastic wave propagation theory, the "safe" maximum impact velocity is directly related to the elastic limit of the incident bar [1]. Such a condition limits the maximum strain rate in the test. Assuming the same mechanical impedances of the striker and the incident bar, the maximum impact velocity (V_m) can be estimated from the relation $V_m = 2\sigma_y/\rho C_0$, where σ_y ,ρ and C_0 are, respectively, the yield stress, the density, and the elastic wave speed in a slender rod. If the striker and the incident bar are of the same yield stress, for example $\sigma_y \approx 2.0$ GPa then $V_m \approx 100$ m/s, then the mass velocity in both bars is $v \approx 50$ m/s. Assuming further that the typical specimen length l_0=8.0 mm, an estimation of the maximum strain rate yields the value $\dot{\varepsilon}_m \approx 6.2*10^3 s^{-1}$. In order to reach higher strain rates than ~10^4 s^{-1}, Dharan and Hauser [11] introduced a modification of the SHPB concept by eliminating the incident bar. Thus, application of the direct impact of a striker onto a small disk specimen supported by the transmitter bar enabled to reach strain rates ~10^5 s^{-1}. Such modification can be defined as the Direct Impact Compression Test (DICT). The removal of the incident bar introduces some difficulty in determining the velocity and displacement as a function of time of the interface between the striker bar and specimen. The axial displacement of the interface specimen-transmitter bar can be determined via the theory of elastic wave propagation. This difficulty was omitted in the first arrangement [11] by the application of a striker with a much larger diameter D_s= 50.8 mm (2.0 in) and a transmitter bar with D_t=9.52 mm (3/8 in), and the ratio D_s/D_t=8.0. Thus, the striker was assumed as being perfectly rigid. With specimen lengths from 6.35 mm to 1.6 mm, the range of strain rates obtained was: $4*10^3$ s^{-1} to $1.2*10^5$ s^{-1}.

It is clear that the elimination of the incident bar and the reduction of the specimen size leads to a substantial increase of the maximum nominal strain rate in DICT experimental technique. By definition, an approximate value of the nominal strain rate is $\dot{\varepsilon}_n = V_0/l_0$, where V_0 is the impact velocity of a striker. Of course, specimen reduction can be applied for both SHPB and DICT arrangements. A specimen reduction must be performed proportionally to the length-to-diameter ratio l_0/d_0, usually ~0.5 due to optimization of friction and inertia effects [3, 12, 13]. As a consequence of the specimen reduction, the whole arrangement, that is SHPB or DICT, must also be reduced. Several attempts to reduce the SHPB size, the striker and both bars, were reported in the past [14–16]. Safford [17] reported another miniaturization of SHPB in 1992. The wave dispersion was taken into account. In general, in elastic bars of small dimensions, the wave dispersion is a secondary effect. A new design and some problems associated with miniaturization were published more recently [18]. Those three examples indicate that miniaturization of the conventional SHPB arrangement enables it to reach maximum strain rate ~$4.5*10^4$ s^{-1}.

The DICT technique offers much higher flexibility in programming of the nominal strain rate due to a wide range of the striker velocity, typically from ~1.0 m/s up to ~150 m/s^{-1}. Impact velocities with the gage length l_0= 1.0 mm yield nominal strain rates from 10^3 s^{-1} to $1.5*10^5$ s^{-1}. A more recent review on the DICT technique [19] provides more details on the theory and advantages of such arrangement. In both cases, namely the conventional and miniaturized DICT arrangements, the technical problem arises regarding how to determine the displacement of the interface striker-specimen as a function of time. This technical problem has been solved in several ways. Some of those cases are discussed below. In addition to the initial assumption that the striker is perfectly rigid [11], the velocity measurement of the opposite face of the striker was applied in the early development of DICT [20, 21]. Also, the striker was assumed as a rigid body. The difficulty in strain measurement in DICT arrangement was avoided by the application of a high-speed camera incorporating an optical system with the image-splitting refraction element and lens [15, 22]. The maximum strain rate ~10^5 s^{-1} attained by further miniaturization of the DICT up to 1.5 mm transmitter bar diameter was also reported in literature [16].

An arrangement to perform jump tests by DICT with abruptly decreased strain rate was introduced by Shioiri et al. [23, 24]. Those authors showed that well-controlled stepwise change in the velocity of the front surface of the striker could be obtained.

Although the DICT, including miniaturization, was developed some decades ago, the concept can be used nowadays with a more advanced instrumentation. For example, in the Laboratory of Physics and Mechanics of Materials (LPMM) in Metz University, France, substantial improvements in this technique have been introduced by applying a two-channel non-contact displacement gage [19, 25]. The main improvement lies in precise measurement of the specimen deformation. Two optical transducers react to the movement of the black and white fields. The specimen is painted in white and end parts of the striker and transmitter bar is painted in black.

Miniaturization of the DICT technique with precise measurement of the net displacement of the specimen interfaces is more difficult. The research project reported in this paper was focused on miniaturization of the DICT arrangement with special attention on precise measurement of stress versus strain at strain rates up to ~10^5 s^{-1}.

Advantages of the DICT Arrangement

The review of the previous papers on the DICT clearly shows many advantages introduced by miniaturization. Among the most important are the following:

1. Shorter specimen length leads to an increase of the nominal strain rate. For specimen length 1.0 mm, the impact velocity to reach the nominal strain rate 10^5 s^{-1} is only 100 m/s.
2. Since the specimen length can be limited, the force equilibrium on both specimen interfaces is reached in a relatively short time. However, in the DICT, a direct verification of the level of the force equilibrium is difficult. One possibility is the application of numerical methods; for example a code of Finite Elements. Another possibility is the application of the symmetric impact [19].
3. A short specimen leads to the reduction of strain gradients caused by plastic waves along the compression direction.
4. Overall, small specimen dimensions reduce the effects of the longitudinal and radial inertia that must be taken into account in the correction analysis of the mean stress in the specimen [3, 11–13].
5. Application of Hopkinson bar (transmitter bar) of a small diameter reduces substantially the geometry dispersion of elastic longitudinal waves that occur in slender rods, reducing at the same time the amplitude of the so-called Pochhammer–Chree vibrations [1, 3, 26].

Recent reviews on new experimental methods of materials testing at high strain rates, including several correction methods of wave dispersion effects in bars and different versions of the direct impact techniques, clearly indicate why miniaturization of dynamic tests is advantageous [19, 27, 28].

The most difficult task in miniaturized DICT is determination the net velocity, or the net displacement, of a small specimen. An exact determination of the net displacement, that is $\Delta l_s = l_{0s} - l_s$, where l_{0s} and l_s are, respectively, the initial and the current specimen length, is crucial in an exact determination of strain. For example, assuming the specimen length l_{0s}=1.0 mm, the displacement to determine deformation ε_s=0.01 is Δl_s=10 μm. Up until now, the best techniques to measure fast displacements were based on optical principles. The optical methods, practically with no time delay, can assure, due to short wave lengths of light, an excellent precision. In the present case, three optical techniques could be applied for the DICT scheme. This one is the so-called LORD (Laser Occlusive Radius Detector) and was applied in determination of the radial displacement of the specimen in SHPB [29]. This technique for direct, non-contact measurement of the radial displacement, and also strain, is based on the shadow principle. The integrated optics produces a sheet of coherent light that can be focused to a thickness of a fraction of millimeter at the specimen. The sheet is orthogonal to the specimen axis. The sensing system consists of a collector lens that integrates all of the incoming light to a silicon PIN photodiode located at its focus. The output of this system consists of a voltage that is proportional to the total amount of light entering the collector lens. The specimen blocks part of the laser sheet, and when the specimen is deformed it occludes the light resulting in a drop of the voltage output from the photodiode. The photodiode signal is calibrated in relation to the radial expansion of the specimen.

Another technique of strain measurement applied in the DICT is based on a two-channel optical gage (extensometer). Such a configuration can detect two longitudinal displacements along the specimen axis [19, 25]. The impact side of striker, as well as a small length of the transmitter bar, is painted in black. The specimens are painted in white, therefore the two-channel displacement transducer can record directly the longitudinal displacements of the striker/specimen and specimen/transmitter bar interfaces. Thus, the specimen strain could be directly determined as a function of time [19, 25]. However, when a specimen is very short, the two-channel displacement transducer cannot be applied because technical difficulties arise due to very small distances between specimen interfaces. The minimum distance for the displacement transducer used in LPMM is 3.0 mm. Therefore in the case of a very short specimen, a shadow measurement of strain, different than the LORD technique, has been developed. The shadow method is described in detail in the next part of this paper.

Novel Miniaturized Arrangement

A new miniaturized DICT is shown schematically in Fig. 1. Modification in the mechanical part, similar to reported earlier [23] lies in an introduction of the decelerator tube 5 in which a small Hopkinson bar 3 with miniature SR gages 4 is inserted. The decelerator tube is mounted in supports 7 slightly ahead of the Hopkinson bar 3 with possibility to change the distance between them. Such configuration permits programming of different plastic deformations of specimens. Both the tube and the bar are attached to the bumper 8. The tube can be exactly adjusted to the axis of striker 2 by special support 6, which prevents vibrations. In Fig. 2, the main details of the miniaturized DICT are shown. The striker (No 2 in Fig. 1) of diameter is slightly lower than that of the decelerator tube (No 5 in Fig. 1) triggers deformation of a small cylindrical specimen until it stops by the decelerator tube. The transmitted elastic wave

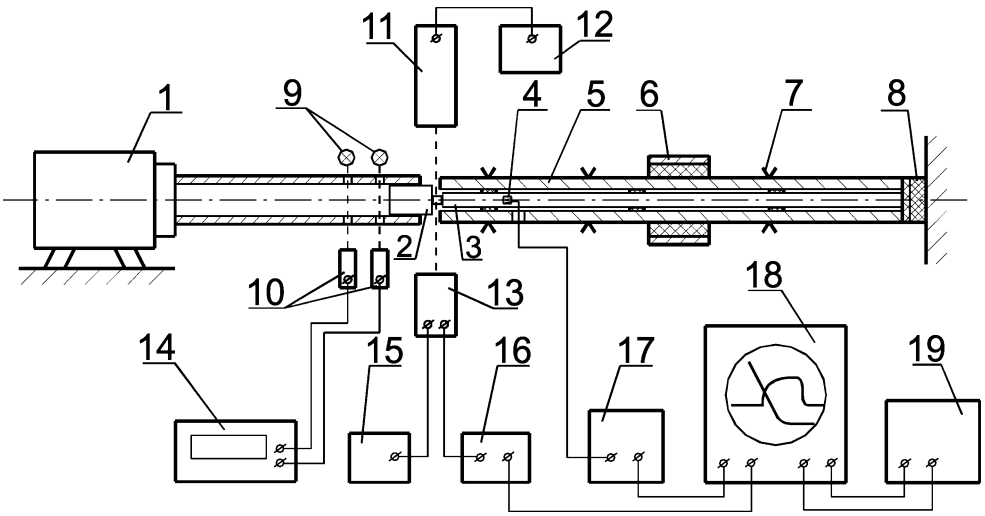

Fig. 1 General scheme of DICT, 1—air gun; 2—striker; 3—transmitter bar; 4—SR gage; 5—decelerator tube; 6—main support; 7—supports; 8—dumper; 9—light sources; 10—photodiodes; 11—laser diode; 12—supply of 11; 13—photodiode (displacement measurement); 14—time counter; 15—supply unit of 13; 16—DC amplifier; 17—SR amplifier; 18—digital oscilloscope; 19—PC

is detected by the SR gage (No 4 in Fig. 1). The net displacement between the striker and the decelerator tube is measured by the shadow technique. Strikers of diameter 11 mm and of different lengths from 12.5 to 50 mm can be launched by an air-gun up to 100 m/s. Specimens of diameter 2.0 mm and lengths from 1.0 to 0.8 mm were supported by the transmitter bar of diameter 5.2 mm and length 243 mm. The transmitter bar was made of maraging steel with the yield stress 2.1 GPa. The relative distance between the tube and the transmitter bar could be varied from 0 up to 2.0 mm. This distance defines the maximum deformation of the specimen. In addition, application of the combination tube–bar enables it to recover specimens after testing, to verify microstructure, for example. The arrangement permits also tests with a negative jump in strain rate [23, 24].

Measurements

The scheme of measurements is shown schematically in Fig. 1. Three independent circuits permit precise measurement of the impact velocity V_0 , the net displacement during specimen deformation $\Delta U(t)=\Delta l_S\ (t)$, and the transmitted elastic wave $\varepsilon_T\ (t)$, where t is time.

The striker is accelerated in the launcher tube 1 of length 840 mm up to pre-programmed impact velocity after pressure calibration, which is $V_0(p)$. The mean impact velocity V_0 is determined by two channels consisting two laser diodes 9, two diaphragms of diameter 0.5 mm, and two photodiodes 10. The perpendicular axis of the laser diodes and photodiodes to the direction of the launcher tube are situated, respectively, 140 and 60 mm from the specimen. Thus, the distance on which the impact velocity is measured is 80 mm. Signals from the photodiodes are recorded by time counter.

The net displacement, and the net mean velocity V_{AV} of specimen deformation, is measured by the principle of shadow, Figs. 1 and 2, and the wave mechanics in the Hopkinson bar. The light emitted by laser diode 11 is formed by a diaphragm and goes through the gap in between the moving striker and the stationary deceleration tube. During the test, the gap is closing up when the specimen is deformed. The displacement of the interface striker/specimen is proportional to the light passed by the gap. The transmitted light is detected by photodiode 13. The photodiode is supplied by unit 15. The electric signal from the photodiode after amplification in 16 is recorded by a two-channel digital oscilloscope 18. It is clear that after calibration, the photodiode voltage can be transformed into the displacement of the interface striker/specimen versus time.

The displacement of the specimen/transmitter bar can be determined via a recording of the signal from the SR. The two SR gages of length 0.6 mm are cemented on the opposite sides of the transmitter bar at the distance of x_g= 35 mm from the specimen end, the aspect ratio x_g/d_H= 6.154, where d_H is the diameter of the transmitter bar. The aspect ratio x_g/d_H ~5.0 is recommended by theoretical as well as numerical analysis of the dynamic St.Venant principle [1, 3, 24, 26]. Assuming the maximum strain rate 10^5 s^{-1}, the velocity of compression is 80 m/s for the specimen length 0.8 mm. Assuming further the maximum nominal strain 0.4 (present case), the period of deformation is T=4.0 μs, therefore the wave length $\Lambda=C_0T$ is in that case 20.0 mm and the aspect ratio is Λ/d_H=3.85, C_0=

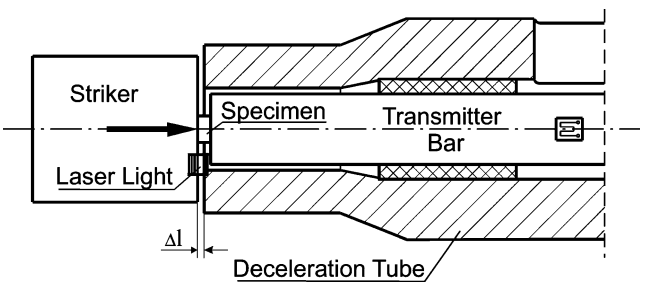

Fig. 2 Zoom of the specimen arrangement

5.0 mm/μs and d_H=5.2 mm. Such extreme conditions constitute the application limit of the theory of elastic waves in slender bars without dispersion.

From the experiment, the following quantities are determined: the impact velocity V_0, the transmitted elastic wave $\varepsilon_T(t)$ and the specimen displacement $\Delta U(t) = U_A(t) - U_B(t)$, where U_A is the displacement of the striker/specimen interface and U_B is the displacement of the specimen/transmitter bar interface. The average velocity of the specimen compression is $V_{AV} = d[\Delta U(t)]/dt$. Having recorded all of those quantities, the specimen strain ε_S (t), the strain rate $\dot{\varepsilon}(t)$, and the mean stress σ (t), all as a function of time, can be calculated by application of the DICT theory.

Theory of the DICT

Although a simplified theory of the DICT has been developed some time ago [11], new points of view can always be added especially on the measurement side [19]. The definitions of the nominal strain rate is given by

$$\dot{\varepsilon}_n(t) = \frac{1}{l_{S0}}\left[\frac{dU_A(t)}{dt} - \frac{dU_B(t)}{dt}\right] \tag{1}$$

where l_{S0} is the initial length of specimen. Since the displacement U_A (t) is measured directly, the velocity $V_A(t)$ can be found by the fist time derivative of U_A (t). The velocity of the specimen/transmitter bar interface can be found from the relation $V_B(t) = \frac{dU_B(t)}{dt}$. This velocity can be found directly via $\varepsilon_T(t)$

$$V_B(t) = C_0\varepsilon_T(t) \tag{2}$$

Thus the nominal strain rate is determined

$$\dot{\varepsilon}_n(t) = \frac{1}{l_{S0}}\left[\frac{dU_A(t)}{dt} - C_0\varepsilon_T(t)\right] \tag{3}$$

An inconvenience is that in order to determine the nominal strain rate, the $U_A(t)$ displacement record must be differentiated. Of course, the nominal strain $\varepsilon_n(t)$ can be found by integration of equation (3), thus

$$\varepsilon_n(t) = \frac{1}{l_{S0}}\left[U_A(t) - C_0\int \varepsilon_T(t)dt\right] \qquad 0 < t < T \tag{4}$$

If strikers are assumed to be rigid during the whole process of specimen deformation, and their kinetic energies are sufficiently high, then deceleration of a striker is zero. Dharan and Hauser [11] assumed the rigid striker in the first version of the DICT. However, it may be assumed that deceleration of the interface A is an increasing function of time, similarly as interaction force $F_A(t)$ between the specimen and the striker. Then, deceleration $a_A = -Bt$, where B is a constant, is determined from the test via $U_A(t)$ record. This procedure eliminates difficulties in finding $V_A(t)$ by the time derivative of $U_A(t)$. Thus, the velocity $V_A(t)$ is given by

$$V_A(t) = V_0 - B\int_0^t \xi d\xi \quad \text{and} \quad V_A(t) = V_0 - \frac{1}{2}Bt^2 \qquad 0 < t < T \tag{5}$$

Assuming that the test is complete in time T, the mean velocity of the interface A is given by

$$\overline{V}_A = \frac{1}{T}\int_0^T \left(V_0 - \frac{1}{2}Bt^2\right)dt \quad \text{and} \quad \overline{V}_A = V_0 - \frac{1}{6}BT^2 \tag{6}$$

From equations (5) and (6) one obtains

$$V_A(t) = V_0 - 3\left(V_0 - \overline{V}_A\right)\left(\frac{t}{T}\right)^2 \tag{7}$$

The parameters in equation (7) V_0, $\overline{V}_A$ and T must be determined from experiment. Approximation of equation (7) taking into account equations (1) and (2) leads to the following formulas for the nominal strain rate

$$\dot{\varepsilon}_n(t) = \frac{1}{l_{S0}}\left[V_0 - 3\left(\left(V_0 - \overline{V}_A\right)\left(\frac{t}{T}\right)^2\right) - C_0\varepsilon_T(t)\right] \tag{8}$$

After integration the nominal strain is obtained

$$\varepsilon_n(t) = \frac{t}{l_{S0}}\left[V_0 - \left(V_0 - \overline{V}_A\right)\left(\frac{t}{T}\right)^2 - \frac{C_0}{l_{S0}}\int_0^t \varepsilon_T(\vartheta)d\vartheta\right] \tag{9}$$

The true strain $\varepsilon(t)$ can be obtained from the standard formula $\varepsilon(t) = |\ln(1 - \varepsilon_n(t))|$.

A simple verification of this procedure is possible by assuming the force equilibrium F_A (t)=F_B (t), then

$$V_A(t) = V_0\frac{1}{m_P}\int_0^t F_B(\xi)d\xi \tag{10}$$

$$V_A(t) = V_0\frac{A_bE_b}{m_p}\int_0^t \varepsilon_T(\xi)d\xi \tag{11}$$

where m_p is the striker mass, A_b and E_b are respectively the cross section of the transmitter bar and its Young's modulus. The values of $V_A(t)$ calculated from equations (10) and (7) on the basis of experimental data exhibit negligible differences. In order to calculate $V_A(t)$ the following data were used: V_0=36.6 m/s, $\overline{V}_A$ = 34.9m/s, T= 8.6*10^{-6} s, m_p=9.38*10^{-3} kg. Level of the assumed force

$F_B(t)$ may be defined as a product of mean stress $\sigma(t)$ presented in Fig. 9 and the area of specimen cross section of initial diameter d_{s0}=2 mm. The maximum difference of $V_A(t)$ values for such experimental data in the entire time period $0<t<T$ does not exceed 2%. In addition the difference between mean values of $V_A(t)$ is only 0.8%. Such differences are small and indicate accurately the procedure applied for determination of $V_A(t)$.

The nominal stress, $\sigma_n(t) \approx F_B(t)/A_{S0}$, in the specimen can be obtained as a function of time, assuming that the force equilibrium occurs during the entire process of specimen deformation. This assumption, which is a good approximation for very short specimens, should be confirmed every time by a FE analysis, for example. In the present case the specimen is very short, l_{S0}=0.8 mm, and the transit time of the elastic wave through the specimen is Δt_S=160 ns. It is well recognized that after 3 to 5 the equilibrium is satisfied [26]. Currently, $3\Delta t_S$=480 ns and this period of time is much shorter than the total time of deformation T=20 μs at strain rate $2*10^4$ s^{-1}. In real tests, the total time of deformation is still longer. The force F_B in the transmitter bar is determined after introduction of the Hook's law

$$F_B(t) = A_b \rho C_0^2 \varepsilon_T(t) \tag{12}$$

where A_b is the cross section area of the transmitter bar. Thus, the average nominal stress $\sigma_n = F_B(t)/A_{S0}$ is given by

$$\sigma_n(t) = \rho C_0^2 \left(\frac{d_H}{d_{S0}}\right)^2 \varepsilon_T(t) \tag{13}$$

where d_{S0} and d_H are, respectively, the initial diameter of specimen, and diameter of the transmitter bar, $d_H > d_{S0}$, ρ is the density of the transmitter bar material. Because all constitutive relations are defined in true values, or true stress, true strain, and true strain rate, it is important to transform the nominal values into the true quantities like $\sigma(t)$, $\varepsilon(t)$ and $\dot{\varepsilon}(t)$. After the elimination of time, the final material characterization can be found: $\sigma(\varepsilon)$ and $\dot{\varepsilon}(\varepsilon)$.

Elimination of Friction, Inertia and Adiabatic Heating

It is well known that friction occurring on the specimen interfaces with platens during a quasi-static compression test increases the mean axial pressure [12, 13, 26, 30]. By the integration of the equation of force equilibrium, several authors estimated in the past the effect of friction at different levels of approximation. For example, Siebel [30] derived an approximate formula for the mean stress on the cylindrical specimen in terms of the axial yield stress

$$\overline{\sigma} = \sigma\left(1 + \frac{\mu d_S}{3 l_S}\right) \quad \text{or} \quad \sigma = \overline{\sigma}\left(1 + \frac{\mu d_S}{3 l_S}\right)^{-1} \tag{14}$$

where $\overline{\sigma}$ and σ are the mean stress determined from experiment and the net flow stress of a material, respectively, μ is the coefficient of Coulomb friction, l_S is the length, and d_S is the specimen diameter. If the coefficient of friction is known, then the flow stress of a material can be found. For example, for specimen dimensions l_S= 1.0 mm, d_S=2.0 mm and μ=0.06 the relative increment of stress is $(\overline{\sigma}/\sigma) - 1 = 0.04$, thus the increase is 4.0%. It is interesting to note that the coefficient of dynamic friction is lower as a rule than the quasi-static one (slow gliding) [31]. Another possibility to reduce the friction effects is application of a ring specimen [32]. Application of ring specimens in dynamic tests was also reported in several papers [11, 15, 33]. In conclusion, the effect of friction in determination of the flow stress in fast compression of specimens having a length to diameter ratio l/d~1 and with a good lubrication is expected to be relatively limited in comparison to other effects, like the radial and longitudinal specimen inertia. However, since the effect of friction may reach a relatively high level for flat specimens of ratio $l/d<$ 0.5, it should be taken into account in determinating the flow stress.

Effects of inertia in DICT are very important because of high accelerations and mass velocities observed in such circumstances. One possibility of estimating the radial inertia is integration of the equilibrium equation in the radial direction and application of the Huber–Mises yield condition [11, 19, 34], then

$$\sigma(t) = \overline{\sigma}(t) - \frac{3}{8}\rho\left(\frac{d_{S0}}{2 l_{S0}}\right)^2 \frac{V^2(t)}{(1 - \varepsilon_S(t))^3} \tag{15}$$

where $V(t)$ is the current axial velocity of specimen compression $V(t) = V_A(t) - V_B(t)$. The second term in equation (15) is the stress correction for the radial inertia.

Another approach to estimation of the inertia effects, axial and radial at the same time, is possible by analysis of the energy balance. Simplified analysis was derived by Davies and Hunter [3] and more exact analyses were reported later [13, 35]. When the energy analysis is applied [3, 13, 35, 36], the following relations are obtained for the pressures σ_A and σ_B on the specimen side A and side B

$$\sigma_A = \sigma - \rho\left(\frac{R_S^2}{8} + \frac{l_S^2}{3}\right)\ddot{\varepsilon} + \rho\left(\frac{R_S^2}{16} - \frac{l_S^2}{3}\right)\dot{\varepsilon}^2 + \frac{\rho l_S \dot{u}}{2} \tag{16}$$

$$\sigma_B = \sigma - \rho\left(\frac{R_S^2}{8} - \frac{l_S^2}{6}\right)\ddot{\varepsilon} + \rho\left(\frac{R_S^2}{16} + \frac{l_S^2}{6}\right)\dot{\varepsilon}^2 - \frac{\rho l_S \dot{u}}{2} \tag{17}$$

where u is the convection velocity. The convection velocity is never very high because the specimen mass is supported all the time by the transmitter bar and its face B moves with

the velocity $V_B=C_0\ \varepsilon_T(t)$which is relatively low. The mean pressure $(\sigma_A+\sigma_B)/2$ minus the flow stress, that is the inertia overstress, is given by

$$\Delta\sigma = \frac{1}{2}(\sigma_A + \sigma_B) - \sigma \tag{18}$$

Thus, the explicit form for the overstress is found

$$\Delta\sigma = -\rho\left(\frac{R_S^2}{8} + \frac{l_S^2}{12}\right)\ddot{\varepsilon} + \rho\left(\frac{R_S^2}{16} - \frac{l_S^2}{12}\right)\dot{\varepsilon}^2 \tag{19}$$

Finally, the pressure difference due to combined effects of specimen strain acceleration and strain rate is found

$$\sigma_A - \sigma_B = -\rho\frac{l_S^2}{2}\left(\ddot{\varepsilon} + \dot{\varepsilon}^2\right) + \rho l_S\dot{u} \tag{20}$$

where ρ is the specimen density, R_S and l_S are, respectively, the current specimen radius and the current specimen length. Definitions of $\dot{\varepsilon}$, $\ddot{\varepsilon}$ are given by:

$$\dot{\varepsilon} = -\frac{V}{l_S} \quad \text{and} \quad \ddot{\varepsilon} = -\left[\frac{1}{l_S}\frac{dV}{dt} + \left(\frac{V}{l_S}\right)^2\right] \tag{21}$$

The early numerical analysis of both friction and inertia in SHPB was reported in 1975 [26]. Currently, many numerical analyses have been published on specimen behavior in high-speed compression and it is out of scope of this paper to review those results.

The most general solutions for both effects the friction and inertia in the form of overstress is given by [12, 37]

$$\Delta\sigma = \frac{\mu\overline{\sigma}}{3s} + \frac{\rho d_S^2}{12}\left(s^2 - \frac{3}{16}\right)\left(\dot{\varepsilon}^2 + \ddot{\varepsilon}\right) + \frac{3\rho d_S^2}{64}\ddot{\varepsilon} \tag{22}$$

where s is the current ratio of the specimen length to the specimen diameter, $s = l_S/d_S$. The effect of the convection velocity is not taken into consideration. The first term appears due to friction and the next two are the results of inertia. The second term vanishes for all specimens satisfying the conditions: $s^2 - 3/6 = 0$, or when $\dot{\varepsilon}^2 + \ddot{\varepsilon} = 0$ which may occur for $t>t_r$, where t_r is the rise time of the initial portion of the transmitted wave $\varepsilon_T(t)$. The ratio $s_D = \sqrt{3}/4$, (s_D=0.433) for Poisson's ratio ν=1/2 was derived as the optimal one by Davies and Hunter [3], but under assumption μ=0. According to equation (22) the stress difference $\Delta\sigma = \overline{\sigma} - \sigma$ shows the absolute minimum and the following s_{opt} is determined as

$$s_{opt} = \left[\frac{2\mu\overline{\sigma}}{\rho d_S^2\left(\dot{\varepsilon}^2 + \ddot{\varepsilon}\right)}\right]^{1/3} \tag{23}$$

Since during the process of specimen deformation, both terms $\mu\overline{\sigma}$, particularly $\dot{\varepsilon}^2 + \ddot{\varepsilon}$, change continuously, a specific value of s_{opt} should be calculated individually for a region of strains and strain rates which are of interest for experimenter. For example, when s_{opt} has been calculated for the present conditions of DICT: $\overline{\sigma} = 1.0$ GPa, ρ=7.8 g/cm^3 (steel), d_S=2.0 mm, μ=0.06,$\dot{\varepsilon} = 2 * 10^4\ s^{-1}$, $\ddot{\varepsilon} = 2 * 10^{10}\ s^{-2}$, the result is s_{opt}=0.57, when $\dot{\varepsilon} = 4.5 * 10^4\ s^{-1}$ and $\ddot{\varepsilon} = 4.5 * 10^{10}\ s^{-2}$, s_{opt}=0.43. The specimens with ratio s equal to 0.5 and 0.4 were used in the fast compression tests. This optimization is only valid around the rise time at the beginning of deformation. At larger mean strain, the mean strain acceleration diminishes substantially (around 100 times) and s_{opt} increases (for example for $\ddot{\varepsilon} = 5 * 10^8\ s^{-2}$ the value of s_{opt} increases to 1.14). At the end of the test the strain acceleration is close to zero and at $\dot{\varepsilon} = 4.5 * 10^4\ s^{-1}$$s_{opt}$=5.7 with l_{S0}=11.4 mm. Of course, such dimensions are not acceptable. Now it is known that there is no one optimal specimen dimension. In fast compression, only an approximate value can be estimated depending on the conditions of experiment.

In conclusion, the inertia, and therefore elastic-plastic wave propagation, cause non-uniformity of stress and strain fields during fast deformation of the specimen. The overstress $\Delta\sigma$ increases when the coefficient of friction is higher, the density increases, the strain rate and strain acceleration are higher, and specimen diameter is larger, equation (22). It has been shown that the most important parameter causing initial oscillations of $\Delta\sigma$, the inertia peak, is the rise time t_r, and its frequency corresponds closely to radial propagation of bulk waves [26]. Since the strain acceleration substantially changes during specimen deformation, generally it increases sharply and next diminishes, or in the case of SHPB can be also negative, variations of $\Delta\sigma(\varepsilon)$ can be quite high in comparison to the mean stress $\overline{\sigma}$. The miniaturization reduces those effects enormously. On the other hand, a very small diameter of Hopkinson bar can reduce oscillations caused by the radial inertia and the wave dispersion during propagation of transmitted waves. This is why the wave dispersion is not discussed in this paper.

One of the most important problems in correct determination of stress–strain characteristics at high and very high strain rates is the thermal softening of specimen material due to adiabatic heating. Due to many publications on this subject, only the most useful in the present analysis are mentioned. When plastic deformation increases, the adiabatic heating due to conversion of plastic work into thermal energy triggers a "closed loop" process of the material softening leading to a decrease of the tangent modulus of stress–strain relation and consequently to a decrease of the flow stress. Because of a positive strain rate sensitivity, the process intensifies at very high strain rates. In the final stages of compression, some forms of mechanical instability appear in the form of Adiabatic Shear Bands (ASB) leading to failure [38–40]. Since at lower strain rates, typically $\dot{\varepsilon} < 10\,s - 1$, plastic

deformation is practically isothermal, in order to compare the adiabatic stress–strain characteristics obtained at higher strain rates than ~10^2 s^{-1} they should be corrected into isothermal conditions [38]. A simple correction procedure applied in this paper is given below [38].

The equation of heat conduction with internal sources applicable to dynamic plasticity is given by

$$\rho C_p \frac{\partial T}{\partial t} = \beta\sigma\left(\varepsilon_p, \dot{\varepsilon}, T\right)\frac{\partial \varepsilon_p}{\partial t} - \lambda\frac{\partial^2 T}{\partial x_1^2} \tag{24}$$

where ρ, C_p, β and λ are, respectively, the density, specific heat, Taylor–Quinney coefficient and thermal conductivity, ε_p and σ are, respectively, the plastic strain and true stress. It can be assumed in fast processes of plastic deformation that the conductivity is zero, λ=0, then the adiabatic deformation occurs and equation (24) is reduced to the ordinary differential equation

$$\frac{dT}{d\varepsilon_p} = \frac{\beta}{\rho(T_0)C_p(T_0)}\sigma\left(\varepsilon_p, \dot{\varepsilon}, T\right) \tag{25}$$

After integration of equation (25)

$$\Delta T_A\left(\varepsilon_p\right)_{\dot{\varepsilon},T} \approx \frac{\beta}{\rho(T_0)C_p(T_0)}\int_0^{\varepsilon_{pm}} \sigma[\xi, T_0]d\xi \tag{26}$$

where $\Delta T_A = T - T_0$ is the temperature increment during adiabatic deformation, T_0 is the initial temperature, and ε_{pm} is the maximal plastic strain under consideration. Here it is assumed that the strain rate is a parameter. In adiabatic conditions, the tangent modulus $(d\sigma/d\varepsilon_p)_A$ versus plastic strain for most of metals and alloys are lower than the isothermal one. Therefore, when the constitutive relation is defined in general form

$$\sigma = f\left(\dot{\varepsilon}, \varepsilon, T\right) \tag{27}$$

$\Delta T_A(\varepsilon_{pm})$ is evaluated from equation (26), the stress difference between isothermal and adiabatic conditions is given by

$$\Delta\sigma = \sigma_T\left(\varepsilon, \dot{\varepsilon}, T_0\right) - \sigma_A\left[\varepsilon, \dot{\varepsilon}, (T_0 + \Delta T_A(\varepsilon))\right] \tag{28}$$

where σ_T and σ_A denote, respectively, the flow stress in isothermal and adiabatic conditions. Thus, from equation (28) the isothermal stress–strain characteristics can be found when the adiabatic curve is obtained from experiment. But in such an approach the constitutive relation, equation (27), must be given in explicit form, which means that all constants should be identified. The simplest method of obtaining an upper bound for $\Delta\sigma$ is to determine experimentally the decrease of flow stress caused by temperature increase ΔT. This is kind of constant for a limited range of temperature at specific values of strain and strain rate is

$$\vartheta = \left(\frac{\partial\sigma}{\partial T}\right)_{\varepsilon,\dot{\varepsilon}}\left[\frac{\text{MPa}}{K}\right] \tag{29}$$

Typical values of the temperature sensitivity ϑ are within the limits [38] −1.0 MPa/K>ϑ>−3 MPa/K and ϑ is of course negative. Then the absolute decrease of stress $\Delta\sigma$ due to adiabatic increase of temperature $\Delta T_A\left(\varepsilon_p\right)_{\dot{\varepsilon},T}$, equation (28), is given by

$$\Delta\sigma\left(\varepsilon_p\right) = \vartheta\ \Delta T_A\left(\varepsilon_p\right)_{\dot{\varepsilon},T} \tag{30}$$

Experimental results for steels indicate that the temperature sensitivity ϑ is approximately constant around room temperature and at temperatures higher that RT, but only for steels without dynamic strain ageing [38]. It appears that ϑ does not depend on strain rate to any great extent. For example, the temperature sensitivity ϑ can be estimated from experimental data reported recently for the annealed 34GS steel tested with SHPB [41]. The results at strain rate 10^3 s^{-1} are shown in Fig. 3 for the range of temperatures from 190 to 470 K. The same steel was tested by DICT and the results are reported in this paper. As expected, the yield stress as well as the flow stress for strain level 0.1, decreases almost linearly with temperature. The temperature sensitivity is relatively low, ϑ≈−0.8 MPa/K. To estimate the adiabatic change of stress $\Delta\sigma$ it may be assumed, as a first approximation, that the flow stress at constant strain rate is a linear function of strain

$$\sigma(\varepsilon)_{\dot{\varepsilon}} = \left(\sigma_y + E_S\varepsilon\right)f\left(\dot{\varepsilon}\right) \quad \text{with} \quad \varepsilon \approx \varepsilon_p \tag{31}$$

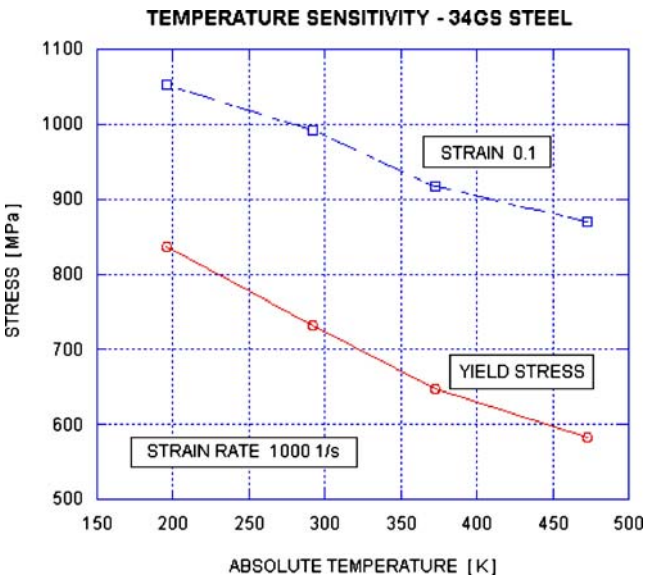

Fig. 3 Effect of temperature on flow stress for two levels of deformation (34GS steel)

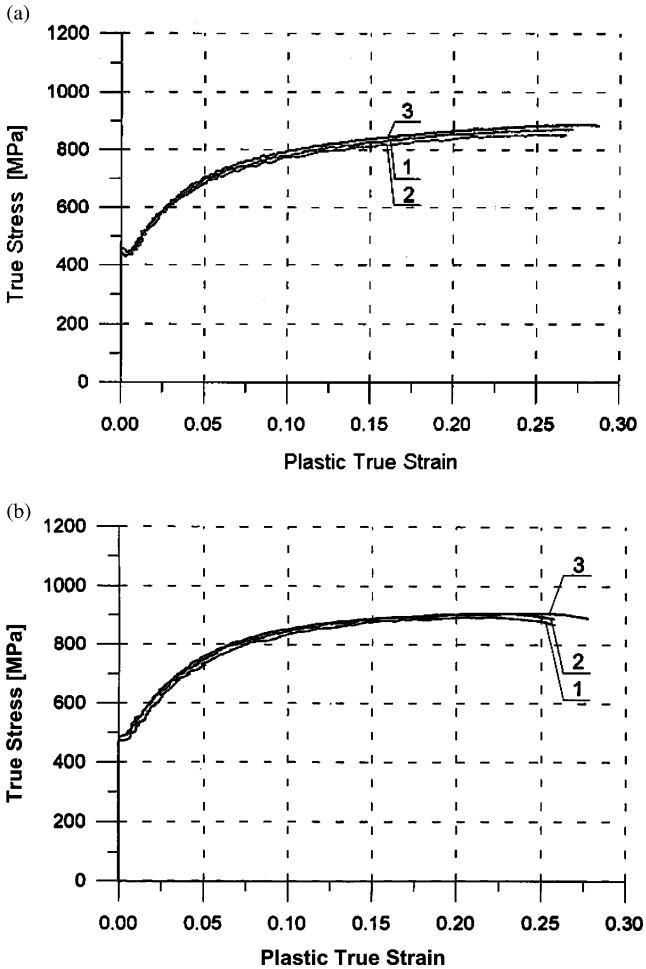

Fig. 4 True stress vs true strain curves for two strain rates (**a**) $\dot{\varepsilon} = 5 * 10^{-4}\,\mathrm{s}^{-1}$; (**b**) $\dot{\varepsilon} = 1.0\,\mathrm{s}^{-1}$

where σ_y and E_S are, respectively, the yield stress and the secant modulus of strain hardening, $f\left(\dot{\varepsilon}\right)$ is unspecified increasing function of strain rate. Substitution of equation (31) into equation (25) yields

$$\Delta T_A(\varepsilon)_{\dot{\varepsilon}} \approx \frac{\beta f\left(\dot{\varepsilon}\right)}{\rho(T_0)C_p(T_0)} \int_0^{\varepsilon} \left(\sigma_y + E_S\xi\right)d\xi \tag{32}$$

The adiabatic increment of temperature after integration of equation (32) is given by

$$\Delta T_A(\varepsilon)_{\dot{\varepsilon}} \approx \frac{\beta f\left(\dot{\varepsilon}\right)}{\rho(T_0)C_p(T_0)} \left(\sigma_y\varepsilon + \frac{1}{2}E_S\varepsilon^2\right) \tag{33}$$

Finally, the stress correction for the adiabatic increase of temperature is obtained in the following form

$$\Delta\sigma(\varepsilon)_{\dot{\varepsilon}} \approx \frac{\vartheta\beta f\left(\dot{\varepsilon}\right)}{\rho(T_0)C_p(T_0)} \left(\sigma_y\varepsilon + \frac{1}{2}E_S\varepsilon^2\right) \tag{34}$$

This equation has been used in further analysis of DICT experiments reported in this paper.

$$\Delta\sigma(\varepsilon)_{\dot{\varepsilon}} \approx \frac{\vartheta\beta\sigma_o\varepsilon f\dot{\varepsilon}}{\rho(T_0)C_p(T_0)} \quad \text{or}$$
$$\Delta\sigma(\varepsilon)_{\dot{\varepsilon}} \approx A(T_0)\sigma_o\varepsilon f\left(\dot{\varepsilon}\right) \tag{35}$$

It can be shown that this approximation is relatively exact for mild steels due to a very limited strain hardening at high strain rates [38]. Of course, the highest decrease of stress due to adiabatic heating occurs for large plastic strains, when the mean stress and the temperature sensitivity are high and the density and the specific heat are low. Since $f\left(\dot{\varepsilon}\right)$ is an increasing function of strain rate the effect of adiabatic heating intensifies at high strain rates.

In conclusion, the correction of the flow stress from adiabatic to isothermal conditions becomes more important at high and very high strain rates. After correction into isothermal conditions the constitutive surface $\left(\sigma, \varepsilon, \dot{\varepsilon}\right)_{To} = 0$ can be determined for any metallic material.

Quasi-static and SHPB Tests of Construction Steel

Compression tests of construction steel 34GS (Polish Standards) were performed at room temperature in as-delivered state at two strain rates, that is $5*10^{-4}$ s^{-1} and 1.0 s^{-1}. Composition of this steel is as follows: (0.3–0.37% C); (0.9–1.2%Mn); (0.6–0.9%Si); $P_{\max}$ −0.05; $S_{\max}$ −0.05. The tests were performed on a servo-controlled universal machine. The specimens of diameter d_S=5.0 mm and of three different initial lengths: l_{S0}=6.5; 4.0, and 2.5 mm permitted for estimation of the effect of friction according to equation (14). The initial aspect ratios s_0 were s_{01}=1.3, s_{02}=0.8 and s_{03}=0.5. The mean $\sigma(\varepsilon_p)$ curves at each strain rate have been obtained as the mean of two compression tests.

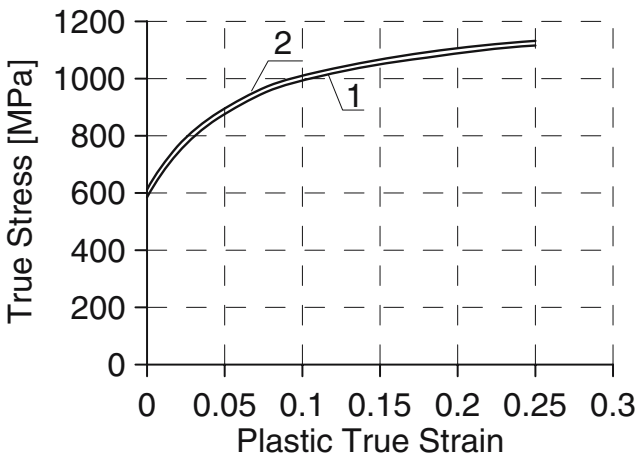

Fig. 5 Mean true stress vs true strain curves for $\dot{\varepsilon} = 10^3\,\mathrm{s}^{-1}$, SHPB data

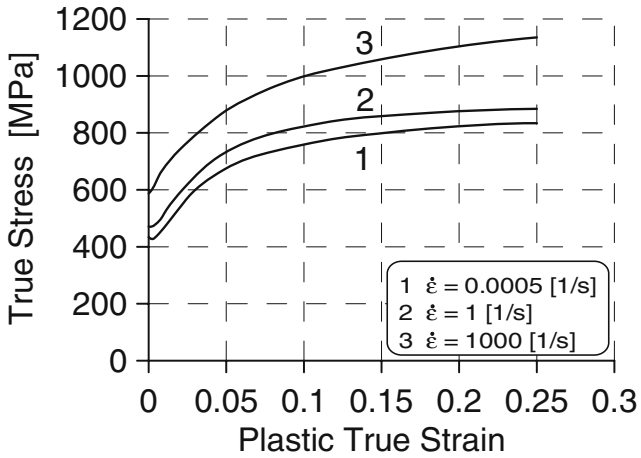

Fig. 6 Comparison of $\sigma(\varepsilon)$ mean curves for three strain rates

Each mean $\sigma(\varepsilon_p)$ curve is adequate to the mean aspect ratio $s_0 = 2s_{01}s_{02}/(s_{01}+s_{02})$, thus $\bar{s}_0 \approx 1.0$. After equation (14) is possible to estimate the stress increment due to friction for each aspect ratio. With lubrication of MoS_2, the relative stress increment due to friction is within the limits from 2 to 2.66% of the mean flow stress for $1.0<s_0<0.75$ and $\mu=0.06$. The complete test results, that is three curves with three aspect ratios for two strain rates $5*10^{-4}$ s^{-1} and 1.0 s^{-1}, are shown respectively in Fig. 4(a) and (b).

Compression tests were performed with the standard SHPB of diameter d_H=15.0 mm with application of the two-wave analysis, that is incident and transmitted waves [4]. The specimen dimensions were d_{S0}=5.0 mm and l_{S0}= 6.5, 4.0, and 2.5 mm. The mean $\sigma(\varepsilon_p)$ curves obtained at strain rate ~10^3 s^{-1} for three above aspect ratios are shown in Fig. 5. Comparison of the mean stress versus plastic strain curves for three strain rates $5*10^{-4}$ s^{-1}, 1.0 s^{-1}, and 10^3 s^{-1} are shown in Fig. 6. The stress–strain curve for 10^3 s^{-1} has been corrected for both friction and adiabatic heating, equations (14) and (30). Thus all curves are transformed into the *isothermal* conditions. It is noted that this construction steel shows substantial strain rate sensitivity as expected for BCC microstructures [9, 25].

Direct Impact Compression Tests

The tests with DICT technique were performed with two high strain rates, that is ~$2*10^4$ s^{-1} and ~$4.5*10^4$ s^{-1}. Those tests permitted not only the evaluation of the technical details of the experimental technique but also to find behavior of the 34GS construction steel within eight orders of strain rate. The specimen dimensions were d_{S0}=2.0 mm and, respectively, l_{S0}=1.0 and 0.8 mm for the lower and the higher strain rate. In Fig. 7, a typical record obtained by the DICT technique is shown. The descending, almost straight, line is the signal from the photodiode showing time evolution of the displacement of the striker–specimen interface A. More exactly, the signal starts after the striker touched the specimen. No substantial deceleration of the striker was observed after the instant of contact. The initial velocity of striker measured by the time counter was V_0= 23.50 m/s and the mean velocity determined from the photodiode record (the mean slope) was V_{av}=21.10 m/s. The time interval of specimen deformation was T=23.70 μs and during that time the interface A was displaced by 0.5 mm. Thus, the absolute value of the maximum true deformation $\varepsilon = |\ln(1-\varepsilon_n)|$ determined from equation (9) was 0.46. The mean strain rate defined as $\dot{\varepsilon} = \varepsilon_m/T$ was $\dot{\varepsilon} = 1.94 * 10^4\,s^{-1}$ The transmitted wave has a typical shape proportional to the nominal stress versus time, equation (13). It may be noted that the time of deformation is shorter by several μs in comparison to the total time of the transmitted wave. This is caused by the fact that the face of the decelerator tube is slightly moving during stopping of the striker. Inserting the precise thin plates and measuring the resulting photodiode voltages performed calibration of the gap between the striker and the decelerator tube. The calibration voltage U [mV] versus the gap between the striker and the decelerator tube Δl [mm] is shown in Fig. 8. The calibration yields a straight line in the range of the gap 0.5 mm>Δl> 0.05 mm.

In Fig. 9, the time histories of stress, strain, and strain rate for the mean strain rate ~$4.5*10^4$ s^{-1} are shown. The specimen was placed 0.3 mm ahead the face of the decelerator tube. The initial and the mean velocities of the interface A were respectively V_0=36.6 and 34.9 m/s. The stress rise time was t_r≈1.1 μs, the total time of deformation was T=8.6 μs, and the true final strain was 0.382. The oscillations of stress, caused by relatively short rise time, trigger the Pochhammer–Chree oscillations due to radial inertia in elastic wave propagation [22, 26, 27]. On the contrary, oscillations in strain rate are relatively small. The main reason is that the mass of the striker, and its kinetic energy, are much higher than the energy needed for the specimen deformation. On the other hand, the

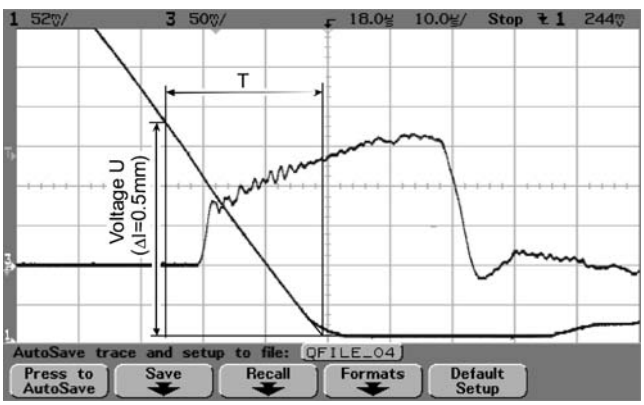

Fig. 7 Digital record of DICT, T is the time of loading

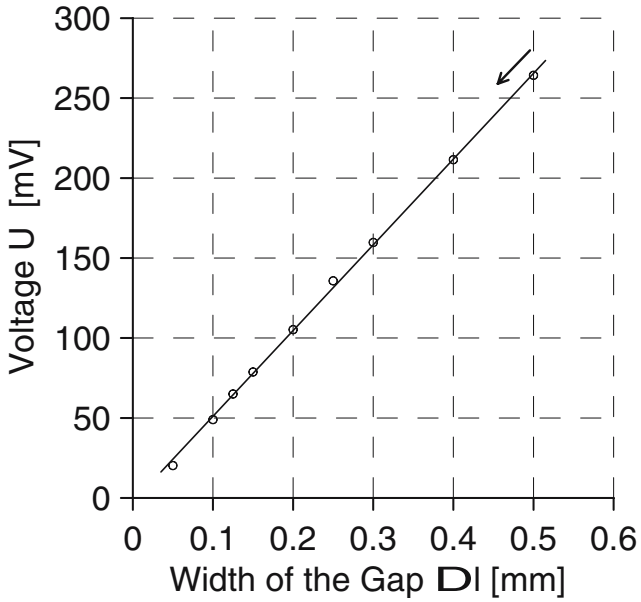

Fig. 8 Displacement calibration

effective mechanical impedance $I_S=A_S\rho C_0$ of the striker is much higher than that of the Hopkinson bar $I_B=A_B\rho C_0$.

Since the time histories of strain rate $\dot{\varepsilon}(t)$ and strain acceleration $\ddot{\varepsilon}(t)$ can be determined for each test the relations (16) and (17) enable estimation of the inertia effects for each interface and the increment of the mean stress due to inertia, equation (18). In the case of miniaturized specimen for the mean strain rate $\dot{\varepsilon} = 4.5 * 10^4\,\mathrm{s}^{-1}$ and the acceleration $\ddot{\varepsilon} = 4.5 * 10^{10}\,\mathrm{s}^{-2}$ the increments of stress due to specimen inertia $\sigma_B-\sigma$ and $\sigma_B-\sigma_A$ are –16.2 and 93 MPa. Theoretical value of the increment of stress $\Delta\sigma$ due to acceleration of the specimen mass center $\dot{V}_{mc} = (V_A + V_B)/2t_r$ is $\Delta\sigma_A$= 124 MPa for $\dot{\varepsilon} = 4.5 * 10^4\,\mathrm{s}^{-1}$ (l_S=0.8 mm, V_A=34.9 m/s, V_B=4.5 m/s and t_r=1.0 μs).

Comparison of all mean curves in the form the true stress vs. true strain obtained at strain rates $5*10^3\ \mathrm{s}^{-1}$, $2*10^4\ \mathrm{s}^{-1}$, and $4.5*10^4\ \mathrm{s}^{-1}$ by the DICT is shown in Fig. 10. All experimental curves have been corrected for the effects of friction and inertia as well as for adiabatic heating, μ=0.06 and ϑ=−0.8 MPa/K. As expected, the effect of friction, the apparent stress is higher than the true flow stress, and the effect of thermal softening, that is the apparent stress is lower than the true flow stress, cancel each other to some extent. For larger strains $0.1<\varepsilon_p<0.4$ both effects superimposed cause stress difference true and apparent not higher than 3.0%. In general, when lubrication is correct the thermal softening dominates, but in the present case the temperature sensitivity ϑ for 35GS steel is relatively low, normally for BCC alloys −1.8 MPa/K<ϑ<−2.6 MPa/K [38].

The set of quasi-static and dynamic $\sigma(\varepsilon)$ curves is shown in Fig. 11. The range of strain rate is from $5*10^{-4}\ \mathrm{s}^{-1}$ to $5*10^4\ \mathrm{s}^{-1}$. All curves are in true coordinates and corrected to *isothermal* conditions with elimination of friction effects. The effect of strain rate on the flow stress is shown in Fig. 12 for four levels of strain. The rate sensitivity $\beta = \left(\partial\sigma \middle/ \partial log\dot{\varepsilon}\right)_{\varepsilon}$ shows two ranges, at lower strain rates $\beta\approx$ 24.6 MPa and $\beta\approx$87.8 MPa above the strain rate threshold $\dot{\varepsilon}_C \approx 50\,\mathrm{s}^{-1}$. Such result suggests existence of two thermally activated dislocation micro-mechanisms of plastic deformation in those two ranges of strain rate [38]. The pseudo-viscosity η defined as $\sigma = \eta\dot{\varepsilon}$, ε=constant has not been found.

Fig. 9 Complete result of DICT at $\dot{\varepsilon} = 4.5 * 10^4\,\mathrm{s}^{-1}$

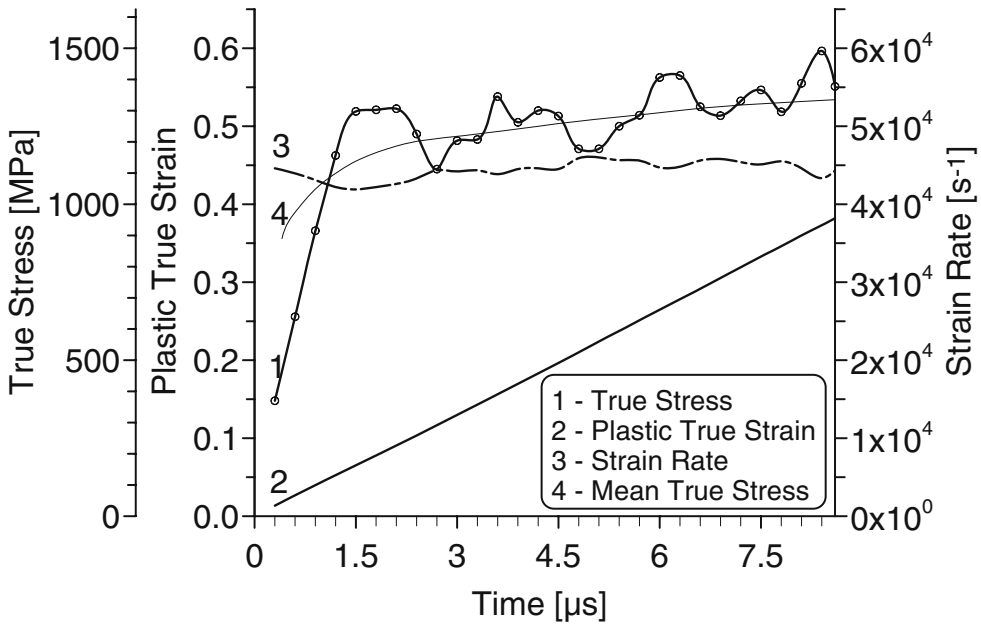

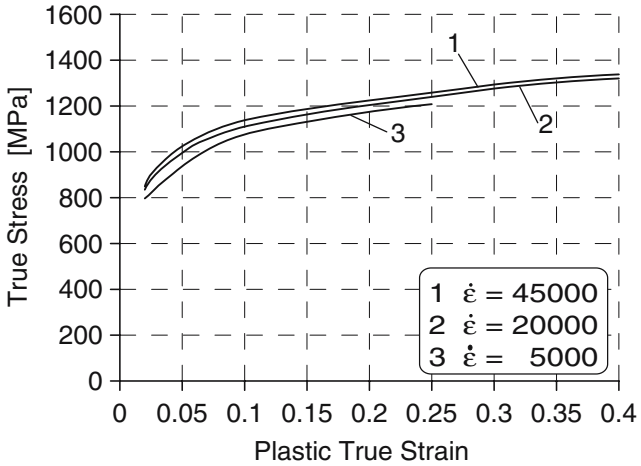

Fig. 10 Mean $\sigma(\varepsilon)$ curves at three strain rates

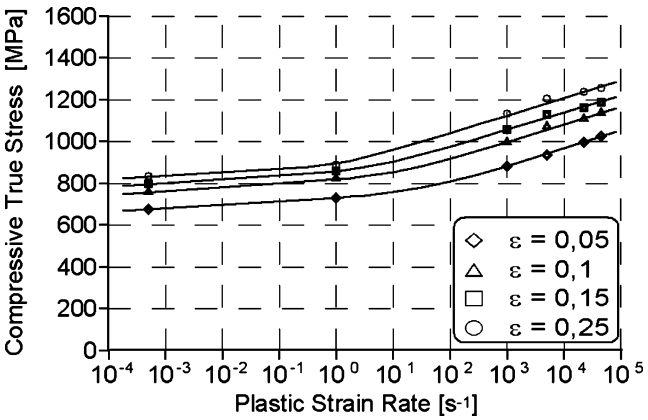

Fig. 12 Rate sensitivity of 34 GS steel at four levels of true strain

Discussion and Conclusions

Introduction of specimen miniaturization in high strain rate materials testing, in both cases SHPB and DICT, enables reaching of high strain rates up to ~10^5 s^{-1}. Typical dimensions applied in miniaturized tests are 1.0 mm<l_{S0}<2.0 mm, 1.0 mm<d_{S0}<2.0 mm and 0.5<s_0< 1.0. Such specimen dimensions reduce substantially the effects of inertia reducing at the same time errors when the inertia analysis is neglected. Although a simple inertia analysis or even FE calculations are recommended, application of very small specimens assures minimum errors in determination of material behavior at very high strain rates. Previous analyses of the inertia effects related to the specimen dimensions indicated that the stress increment due to inertia rises rapidly with strain rate and with specimen dimensions [42]. The strain rate threshold from the thermally activated rate sensitivity to the so-called pseudo-viscosity [9, 11] must be carefully evaluated in the future. Specimen miniaturization on the other hand leads to limitation of grain number in small specimens. For example, if the specimen volume is v_s=2.51 mm^3 (d_S= 2.0 mm and l_S=0.8 mm) and the mean grain diameter is 0.1 mm then the volume of each grain is v_{gr}= $5.23*10^{-4}$ mm^3 and the number of grains in the specimen volume is $N \approx 4.8*10^3$.

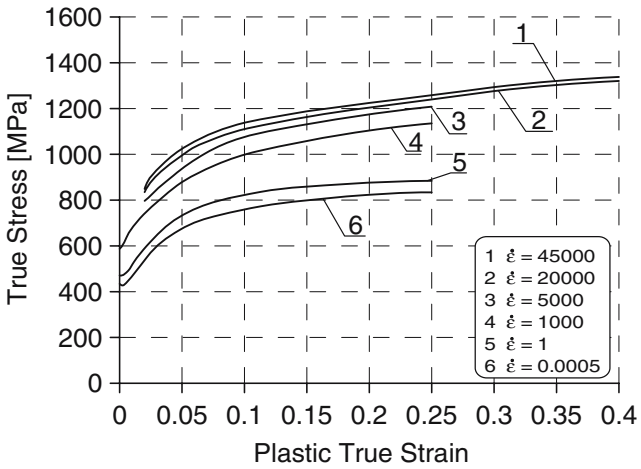

Fig. 11 Comparison of all mean true stress vs. true strain curves for 34 GS steel

Application of small diameter Hopkinson bars substantially reduces dispersion of elastic waves. Because in DICT technique strain gages are cemented closely to the specimen-bar interface, recommended distance ~5 d_H , where d_H is diameter of Hopkinson bar, the transmitted wave is not much distorted in comparison to the signal originating in that interface. In addition, the bar vibration in the longitudinal mode superimposed on the transmitted wave is relatively low [3]. However, it is impossible to monitor the force equilibrium, that is $F_A(t)$ and $F_B(t)$ as a function of time, and the force equilibrium must be assumed. One possibility is an analytic estimation or analysis by a FE (Finite Element) code. Because specimens applied in the miniaturized DICT are short, the stress gradients within a typical specimen are assumed to be small.

In the version of the DICT arrangement reported in this paper, the original and not expensive optical technique to measure displacement of the interface striker–specimen has been applied. Therefore, the combination of the opto-electronic measurement of the displacement of interface A and the theory of elastic wave propagation enabling measurement of the displacement of interface B, has provided an exact measurement of the specimen strain and strain rate as a functions of time.

Combination of the quasi-static precision compression test, with the application of SHPB along with the miniaturized DICT, makes possible the determination of the rate sensitivity of materials for very wide strain rate spectrum, from $5*10^{-4}$ s^{-1} to $5*10^4$ s^{-1}.

Acknowledgements The research reported in this paper was supported in part by the Project KBN (Poland) Nr 7 T07A 02118 (ZM and ZLK) and in part by the Laboratory of Physics and Mechanics of Materials, UMR-CNRS, Metz, France (JRK).

References

1. Kolsky H (1949) An investigation of the mechanical properties of materials at very high rates of loading. Proc Phys Soc London 62B:676.
2. Lindholm US (1964) Some experiments with the Split Hopkinson Pressure Bar. J Mech Phys Solids 12(5):317.
3. Davies EDH, Hunter SC (1963) The dynamic compression testing of solids by the method of the Split Hopkins Pressure Bar. J Mech Phys Solids 11:155.
4. Lindholm US, Yeakley LM (1965) Dynamic deformation of single and polycrystalline aluminum. J Mech Phys Solids 13:41.
5. Harding J, Wood EO, Cambell JD (1960) Tensile testing of materials at impact rates of strain. J Mech Eng Sci 2:88.
6. Nicholas T (1981) Tensile testing of materials at high rates of strain. Exp Mech 21:177.
7. Duffy J, Campbell JD, Hawley RM (1971) On the use of a torsional Split Hopkinson Bar to study rate effects in 1100-0 aluminum. J Appl Mech 93(3):83.
8. Senseny PE, Duffy J, Hawley RM (1978) Experiments on strain rate history and temperature effects during the plastic deformation of close-packed metals. J Appl Mech Trans ASME 45:60.
9. Campbell JD, Ferguson WG (1970) The temperature and strain - rate dependence of the shear strength of mild steel. Phila Mag 81:63.
10. Harding J, Huddart J (1979) The use of the double–notch shear test in determining the mechanical properties of uranium at very high rates of strain. In: Proc. conf. on mech. prop. at high rates of strain, conf. ser. no. 47, Oxford, March, 49.
11. Dharan CKM, Hauser FE (1970) Determination of stress - strain characteristic at very high strain rates. Exp Mech 10:370.
12. Malinowski JZ, Klepaczko JR (1986) A unified analytic and numerical approach to specimen behaviour in the SHPB. Int J Mech Sci 28:381.
13. Gorham DA, Pope PH, Cox O (1984) Sources of error in very high strain rate compression tests. In: Proc. conf. on mech. prop. at high rates of strain, Oxford, conf. ser., 70, 151.
14. Lindholm US (1978) Deformation maps in the region of high dislocation velocity. In: Proc. IUTAM symposium on high velocity deformation of solids, Tokyo, 1977. Springer, Berlin Heidelberg New York, p 26.
15. Gorham DA (1979) Measurement of stress–strain properties of strong metals at very high rates of strain. In: Proc. conf. on mech. prop. at high rates strain, conf. ser. no. 47, Oxford, March, 16.
16. Kamler F, Niessen P, Pick RJ (1995) Measurement of the behavior of high purity copper at very high rates of strain. Can J Phys 73:295.
17. Safford NA (1992) Materials testing up to 10^5 s^{-1} using a miniaturized Hopkinson Bar with dispersion corrections. In: Proc. 2nd intl. symp. on intense dynamic loading and its efects, Sichuan University Press, Chengdu, China, 378.
18. Jia D, Ramesh KT (2004) A rigorous assessment of the benefits of miniaturization in the Kolsky bar system. Exp Mech 44:445.
19. Klepaczko JR (2002) Advanced experimental techniques in materials testing. In: New experimental methods in material dynamics and impact, Inst. Fund. Technological Res., Polish Academy of Sciences, Warsaw, 223.
20. Wulf GL, Richardson GT (1974) The measurement of dynamic stress–strain relationships at very high strains. J Phys E: Sci Instrum 7:167.
21. Wulf GL (1974) Dynamic stress–strain measurements at large strains. In: Mechanical properties at high rates of strain, conf. ser. no 21. The Inst. Phys. London, 48.
22. Gorham DA (1983) A numerical method for the correction of dispersion in pressure bar signals. J Phys E: Sci Instrum 16:477.
23. Shioiri J, Sakino K, Santoh S (1966) Strain rate sensitivity of flow stress at very high rates of strain. In: Kawata K, Shioiri J (eds) IUTAM symp. constitutive relation in high/very high strain rates. Springer, Berlin Heidelberg New York, p 49.
24. Sakino K, Shioiri J (1991) Dynamic flow stress response of aluminum to sudden reduction in strain rate at very high strain rates. J Phys IV, Colloque C3, France, 1, C3/35.
25. Ostwald D, Klepaczko JR, Klimanek P (1997) Compression tests of polycrystalline α- iron up to high strains over a large range of strain rates. J Phys IV, Colloque C3, France, 7, C3/385.
26. Bertholf LD, Karnes CH (1975) Two dimensional analysis of the Split Hopkinson Pressure Bar system. J Mech Phys Solids 23:1.
27. Gary G (2002) Some aspects of dynamic testing with wave-guides. In: New experimental methods in material dynamics and impact, Inst. Fund. Technological Res., Polish Academy of Sciences, Warsaw, 179.
28. Gary G, Klepaczko JR, Zhao H (1991) Correction de dispersion pour l'analyse des petites déformations aux barre de Hopkinson. J Phys III, Colloque C3, France, 1, C3/403–C3/411.
29. Ramesh KT, Narasimhan S (1996) Finite deformations and the dynamic measurement of radial strains in compression Kolsky bar experiments. Int J Solids Struct 33:3723.
30. Siebel E (1923) Grundlagen zur Berechnung des Kraft und Arbeitbedorf bei Schmieden und Walzen. Stahl und Eisen 43:1295.
31. Montgomery RS (1976) Friction and wear at high sliding speeds. Wear 36:275.
32. Avitzur B (1964) Forging of hollow discs. Isr J Technol 2(3):295.
33. Ashton M, Perry DJ (2000) A constitutive relationship for metals compensated for adiabatic and friction effects. In: Proc. 6th int. conf. on mechanical and physical behaviour of materials under dynamic loading, Kraków, 263.
34. Klepaczko JR, Hauser FE (1969) Radial inertia in compression testing of materials. Technical report (internal), Division of Inorganic Materials, University of California, Berkeley.
35. Samanta SK (1971) Dynamic deformation of aluminum and copper at elevated temperatures. J Mech Phys Solids 19:117.
36. Klepaczko J, Malinowski Z (1978) Dynamic frictional effects as measured from the Split Hopkinson Pressure Bar. In: Kawata K, Shioiri J (eds) Proc. IUTAM symposium on high velocity deformation of solids, Tokyo, 1977. Springer, Berlin Heidelberg New York, p 63.
37. Malinowski JZ (1987) Cylindrical specimen compression analysis in the Split HopkinsonPressure Bar system. Eng Trans 35(4):551.
38. Klepaczko JR, Duffy J (1982) Strain rate history effects in body-center-cubic metals. ASTM-STP 765:251.
39. Klepaczko JR (1968) Generalized conditions for stability in tension test. Int J Mech Sci 10:297.
40. Semiatin SL, Jonas JJ (1984) Formability and workability of metals. ASM, Metals Park, OH.
41. Kruszka L (2004) Behaviour of structural steel at high strain rates and at elevated and low temperatures. In: Proc. ISIE-5, University of Cambridge, UK, (poster).
42. Gorham DA (1991) An effect of specimen size in the high strain rate compression test. Proc. Conf. Dymat, Coll. C3, suppl. Journal de Physique III, 1, C3–411.